Journal of Crystal Growth ∎ (∎∎∎∎) ∎∎∎–∎∎∎

Contents lists available at ScienceDirect

Journal of Crystal Growth

journal homepage: www.elsevier.com/locate/jcrysgro

Theoretical and experimental study of highly textured GaAs on silicon using a graphene buffer layer

Yazeed Alaskar [a,b,1], Shamsul Arafin [a,1], Qiyin Lin [c], Darshana Wickramaratne [d], Jeff McKay [e], Andrew G. Norman [f], Zhi Zhang [g], Luchi Yao [h], Feng Ding [i], Jin Zou [g], Mark S. Goorsky [e], Roger K. Lake [d], Mark A. Zurbuchen [a], Kang L. Wang [a,*]

[a] Device Research Laboratory, Department of Electrical Engineering, University of California at Los Angeles, CA 90095, USA
[b] National Nanotechnology Research Center, King Abdulaziz City for Science and Technology, Riyadh 11442, Saudi Arabia
[c] Laboratory for Electron and X-ray Instrumentation, University of California at Irvine, CA 92697, USA
[d] Laboratory for Terahertz and Terascale Electronics, Department of Electrical and Computer Engineering University of California at Riverside, CA 92521, USA
[e] Department of Materials Science and Engineering, University of California at Los Angeles, CA 90095, USA
[f] National Renewable Energy Laboratory, Denver, CO 80401, USA
[g] Materials Engineering, The University of Queensland, St. Lucia, Qld 4072, Australia
[h] Shanghai Institute of Technical Physics, Chinese Academy of Science, Shanghai 200083, China
[i] Institute of Textiles and Clothing, Hong Kong Polytechnic University, Hong Kong, China

ARTICLE INFO

Keywords:
A3. Thin film
A3. Molecular beam epitaxy
B2. Semiconducting gallium arsenide
B2. Semiconducting III-V materials
B2. Semiconducting silicon

ABSTRACT

A novel heteroepitaxial growth technique, quasi-van der Waals epitaxy, promises the ability to deposit three-dimensional GaAs materials on silicon using two-dimensional graphene as a buffer layer by overcoming the lattice and thermal expansion mismatch. In this study, density functional theory (DFT) simulations were performed to understand the interactions at the GaAs/graphene hetero-interface as well as the growth orientations of GaAs on graphene. To develop a better understanding of the molecular beam epitaxy-grown GaAs films on graphene, samples were characterized by x-ray diffraction (θ–2θ scan, ω-scan, grazing incidence XRD and pole figure measurement) and transmission electron microscopy. The realizations of smooth GaAs films with a strong (111) oriented fiber-texture on graphene/silicon using this deposition technique are a milestone towards an eventual demonstration of the epitaxial growth of GaAs on silicon, which is necessary for integrated photonics application.

1. Introduction

Since the proposed concept and first experimental realization [1], van der Waals epitaxy (vdWE) has gained significant momentum within the research community. Recently, vdWE is viewed as a prospective alternative route of heteroepitaxy by which heterostructures even with a lattice mismatch of as high as 40% can be grown with reasonably good crystal quality [2]. Although the original concept of vdWE was realized using two-dimensional (2D) layered semiconductors, such as $NbSe_2/MoS_2$; the growth of three-dimensional (3D) materials on top of a 2D surface is an extension of this growth idea [3]. This modification of vdWE is often referred to as quasivan der Waals epitaxy (QvdWE) or 3D–2D heteroepitaxy [4].

The epitaxial growth of optoelectronic materials, such as GaAs on silicon substrates, provides a unique opportunity to combine the advantages of superior optical properties with the capabilities of matured silicon technologies. Despite extensive efforts over the last 30 years, there has been little success in the growth of high-quality GaAs on Si. The main obstacles are lattice mismatch, polar-on-nonpolar epitaxy, and thermal expansion mismatch between GaAs and Si [5,6]. Due to such intrinsic material-related problems, the grown GaAs thin films on Si are still far below the technologically acceptable limit, resulting poor performance in the devices made of such materials. In this regard, QvdWE could be considered as a method to overcome such problems. This technique employs layered two-dimensional materials as buffer layers which are self-passivated and inert, indicating a weak vdW interaction between the overlying–3D–semiconductor and the 2D-layer.

Among the large family of vdW materials, graphene, a single layer of sp^2-bonded carbon atoms, a thermally-stable material with high-decomposition temperature, could be an ideal choice as buffer layer material. Furthermore, due to its excellent optical

* Corresponding author.
E-mail addresses: sarafin@ucla.edu (S. Arafin), wang@seas.ucla.edu (K.L. Wang).
[1] These authors contributed equally to this work.

http://dx.doi.org/10.1016/j.jcrysgro.2015.02.003
0022-0248/

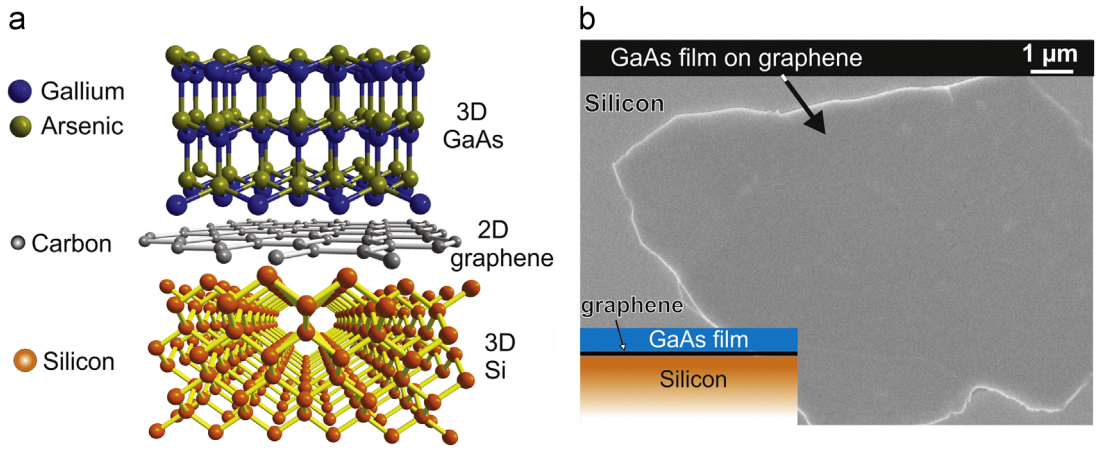

Fig. 1. (a) Atomic geometry of GaAs/graphene/Si, where GaAs and graphene are attached to each other by van der Waals interactions. (b) SEM plan-view image of the as-grown GaAs thin films on graphite flakes exfoliated atop Si (001) substrates, showing a smooth surface morphology.

transparency and electrical conductivity, graphene is a promising substrate for GaAs-based optoelectronic devices [7,8]. Hence, low-resistive, transparent and flexible ohmic contact could be formed on those devices.

A few experimental investigations [4,9,10] have already been reported on the growth of GaAs nanowires on Si using graphene. However, successful operation of nanowire-based devices is impeded by several intrinsic challenges which are primarily associated with the cylindrical geometry of NWs [11]. Thus far, nanowires still have not turned out to be the proper alternative of thin-film, when optical and electrical device characteristics are considered.

Using a 2D graphene buffer layer, the epitaxial growth mode of 3D GaAs materials on silicon substrate is shown schematically in Fig. 1(a) through a covalent bond diagram of the corresponding materials. GaAs which has a zinc-blende cubic crystal structure interacts with the underlying graphene layer with a honeycomb lattice structure via vdW forces. Fig. 1(b) shows an SEM image of molecular beam epitaxy (MBE) grown smooth GaAs films grown on gallium-terminated graphitic flakes lying on silicon substrate. Despite an ultrasmooth morphology of such GaAs films, the low adsorption and migration energies of gallium and arsenic atoms on graphene result in cluster-growth mode during crystallization of GaAs films at an elevated temperature. Details on the growth process and the associated physics can be found elsewhere [12].

2. Theoretical investigation

Density functional theory (DFT) calculations within the Perdew–Burke–Ernzerhof (PBE) type generalized gradient approximation (GGA) framework as implemented in the Vienna Abinitio Simulation Package (VASP) [13] were performed. Using a semi-empirical correction to the Kohn–Sham energies, vdW interactions were accounted for in all calculations [14]. A Monkhorst–Pack scheme was adopted to integrate over the Brillouin zone with a *k*-mesh $9 \times 9 \times 1$. A plane-wave basis kinetic energy cutoff of 400 eV was used. All structures are optimized until the largest force on the atoms is less than 0.01 eV/Å.

2.1. VdW hetero-interface study

The interface between zinc-blende (ZB) and wurtzite (WZ) GaAs on graphene is compared using ab-initio calculations. A $4 \times 4 \times 1$ graphene supercell is used with a $5 \times 5 \times 1$ GaAs supercell. The graphene/GaAs interfaces are Ga terminated. To saturate the dangling bonds pseudo-hydrogen atoms with fractional charge of 0.75e were used. The binding energy $E_{binding}$ is calculated using the following expression:

$$E_{binding} = E_{graphene/GaAs} - E_{graphene} - E_{GaAs}$$

where $E_{graphene/GaAs}$ is the ground state energy of the graphene/GaAs heterostructure, $E_{graphene}$ is the ground state energy of the $4 \times 4 \times 1$ graphene supercell and E_{GaAs} is the ground state energy of the GaAs supercell.

Table 1
Binding energy values of zinc-blende and wurtzite GaAs surfaces on graphene.

	Binding energy/C atom (meV)	
	Zinc blende GaAs (111)	**Wurtzite GaAs**
Pristine	−43.21	−35.11
Ga-vacancy	−43.18	−33.98

To understand the nature of the heterointerface, the binding energy between graphene and the ZB and WZ GaAs surfaces is calculated. The binding energy describes the strength of the interactions at the epitaxial interface. Table 1 summarizes the binding energies between ZB GaAs (111) surface and WZ GaAs (0001) surface with graphene. The energies for a pristine interface and in the presence of a single point defect are compared. A point defect is introduced with the removal of a single Ga atom at the Ga-terminated graphene/GaAs interface.

Calculations of the binding energy indicate the ZB GaAs (111) phase is the preferred orientation on graphene; the ground state energy for this configuration is 8.1 meV/C-atom lower than the energy of WZ GaAs phase on graphene. With the presence of a single point-defect at the interface; the ZB GaAs phase remains the preferred orientation. Prior studies have demonstrated that the epitaxial relationship formed by GaAs and graphene can be affected by but is not limited to the orientation, strain, defect density at the interface [4]. Further calculations would elucidate which of these mechanisms governs the preferred GaAs phase when epitaxially grown atop graphene.

Interfaces dominated by vdW forces are known to lead to turbostratically misoriented interfaces. Hence, the effect of misorientation between the graphene–GaAs interface on the binding energy is also investigated. The binding energy is maximum for the misoriented structure and is minimum for the unrotated graphene/GaAs structure. The binding energies calculated as a function of rotation angle in Fig. 2 are the same order of magnitude as the binding energy of graphene on Cu (111) surfaces [15], where the interactions at this interface are also dominated by vdW forces. This

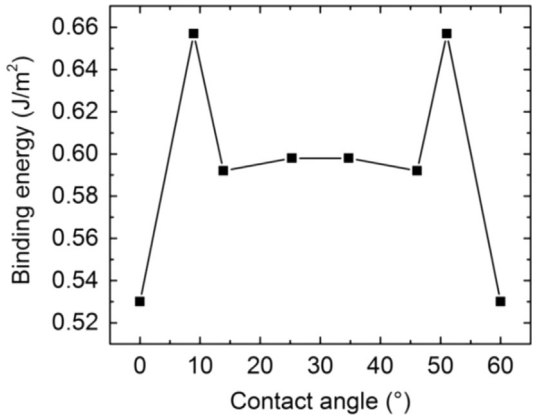

Fig. 2. Binding energy of the graphene/GaAs interface as a function of misorientation angle. The calculated binding energies are normalized with the planar area of the supercell used.

would also suggest that the graphene–GaAs interface is also governed by vdW interactions. The stronger binding energy in the misoriented structure suggests the strain in this structure is minimized. Furthermore, the higher binding energy would also suggest that the graphene–GaAs interface is likely to be misaligned when an epitaxial interface is formed, with an unrotated interface being the least preferred orientation configuration. The energy barrier to transition from a rotated interface to an unrotated interface in the graphene/GaAs structure can be as large as 0.13 J/m^2. For the supercells simulated, the total energy difference between the unrotated structure and the rotated structures is greater than the thermal energy k_BT at room temperature. This would suggest the interface between graphene and GaAs may remain misaligned at 300 K and higher growth temperatures as well.

2.2. Alternative QvdWE buffer layer materials

As wafer-scale growth of single monolayers of alternative vdW materials, such as h-BN and MoS_2 [16] approach the same quality as graphene, we consider the possibility of using these prototypical vdW materials as a buffer layer for our quasi-vdW epitaxy approach. Adsorption energy calculations were used to determine if monolayer and bilayer MoS_2 and h-BN would act as suitable buffer layers (in addition to graphene) to achieve QvdWE of GaAs. For calculations of the adsorption energy of Ga, Al, In and As on hBN and MoS_2, a $4 \times 4 \times 1$ supercell of monolayer (1L) MoS_2 and monolayer and bilayer (2L) hBN was used. For MoS_2, the 4p, 5s, 4d and 3s, 3p orbitals of Mo and S respectively are treated as valence in the PBE functional. For h-BN, the 2s, 2p orbitals of B and N are treated as valence. Calculation details for the adsorption energy and the Ga, Al, As and In pseudo-potentials used have been detailed in our previous study of adsorption energy of these elements on graphene [12]. Our prior studies of Al, Ga, As and In adsorption on graphene have shown that each element binds with approximately the same binding energy on to single layer and bilayer graphene; the favored binding site on the honeycomb lattice of graphene is unique to each element. Hence, the binding energy of the defect free GaAs surface is determined by the orientation of the Ga and As atoms above the honeycomb lattice. Table 2 summarizes the adsorption energy values for Al, Ga, As and In on h-BN and MoS_2.

The adsorption energy at each binding site for monolayer MoS_2 and monolayer and bilayer h-BN is approximately an order of magnitude lower than the adsorption energies calculated for Ga, Al, In and As on graphene. The strength of the adsorption energy can be characterized by the hybridization of the adsorbant elements on the vdW buffer layer material. Fig. 3 illustrates the projected

Table 2
Adsorption energy of Ga, Al, In and As on monolayer (1L) and bilayer (2L) h-BN and MoS_2. The favored adsorption site for each element and vdW material is listed in parentheses; for h-BN the favored site is when the adatom is on top of nitrogen (TN) or on top of the boron–nitrogen bond (B) and for MoS_2 the favored site is when the adatom is on top of the sulfur atom (T).

Adsorption energy			
	1L h-BN (meV/atom)	**2L h-BN (meV/atom)**	**1L-MoS_2 (meV/atom)**
Ga	131.6 (TN)	134.3 (TN)	234.6 (T)
Al	135.1 (TN)	101.1 (TN)	237.4 (T)
In	66.9 (B)	85.1 (TN)	573.1 (T)
As	296.9 (B)	341.5 (TN)	527.8 (T)

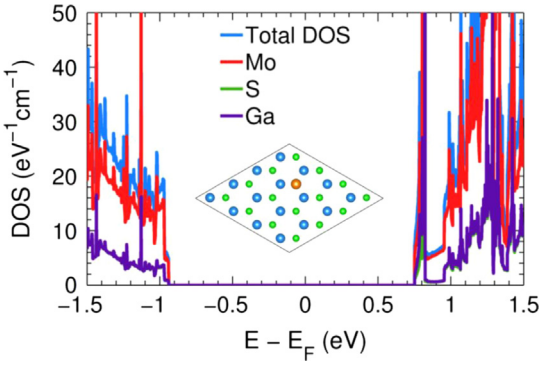

Fig. 3. Projected density of states for Ga adsorbed on the T-site of the MoS_2 supercell, total density of states (blue), Mo states (red), S states (green) and Ga states (magenta). Inset: Schematic of $4 \times 4 \times 1$ MoS_2 supercell with Ga adatom over S atom. (For interpretation of the references to color in this figure legend, the reader is referred to the web version of this article.)

density of states of a Ga atom adsorbed on the T-site of a monolayer MoS_2 supercell. The sp^2 orbitals of Ga are weakly hybridized with the 4d and 3p orbitals of Mo and S respectively. This is evidenced by the weak overlap of the Ga orbitals with the Mo and S orbitals of the valence band in MoS_2. In contrast, strong hybridization between the sp^2 orbitals of Ga with the sp^2 orbitals of carbon in graphene results in larger adsorption energies. The adsorption of Ga, Al, In and As atoms on 1L and 2L h-BN also results in weak hybridization with the sp^2 orbitals of boron and nitrogen which leads to lower adsorption energies when compared to graphene. The lower adsorption energies of Ga, Al, As and In atoms on the MoS_2 and h-BN surfaces would result in these adatoms being poorly anchored during the growth process, which in turn would lead to degradation in the morphology of the GaAs film. These initial calculations suggest that graphene remains an ideal candidate as a buffer material to enable vdW epitaxy when compared to h-BN and MoS_2.

3. Experimental procedure

X-ray diffraction experiments were performed at room temperature on a Rigaku SmartLab diffractometer equipped with a high accuracy/resolution four circle theta–theta goniometer, using a Cu Kα radiation and scintillation detector. The nearly parallel incident beam was collimated using a parabolic multilayer mirror. Sample was mounted horizontally on a motorized high precision Z-stage and Phi attachment. Full pole figure data was collected using an in-plane diffraction attachment with the axis β scanned from 0° to 360° at 50°/min speed at each α angle (step size 0.5° ranging from 0° to 90°). The incident slit (IS), length limit silts (H), and receiving slits (RS1/RS2) were 1 mm, 5 mm, 2 mm and 2 mm, respectively. For grazing

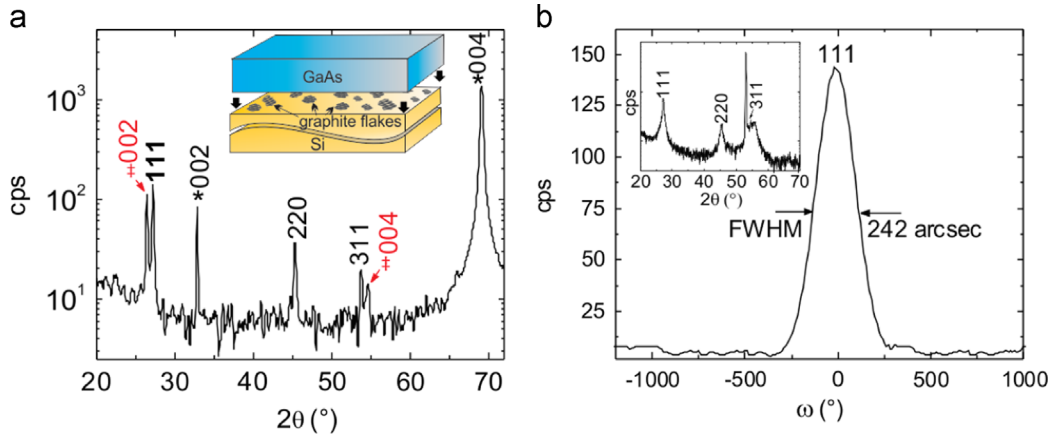

Fig. 4. XRD analyses of as-grown GaAs on exfoliated graphite flakes, (a) HRXRD θ–2θ scan, where multiple peaks correspond to zinc–blende (111), (220) and (311) GaAs, confirming polycrystallinity of the grown films. The (002) and (004) graphite peaks marked with doubledaggers (‡) indicate the multidomain graphite layers. The (002) and (004) peaks from Si (001) substrate are marked with asterisks (*). (b) The rocking curve of (111) GaAs peak, GIXRD 2θ scan profiles are shown in the inset. (For interpretation of the references to color in this figure, the reader is referred to the web version of this article.)

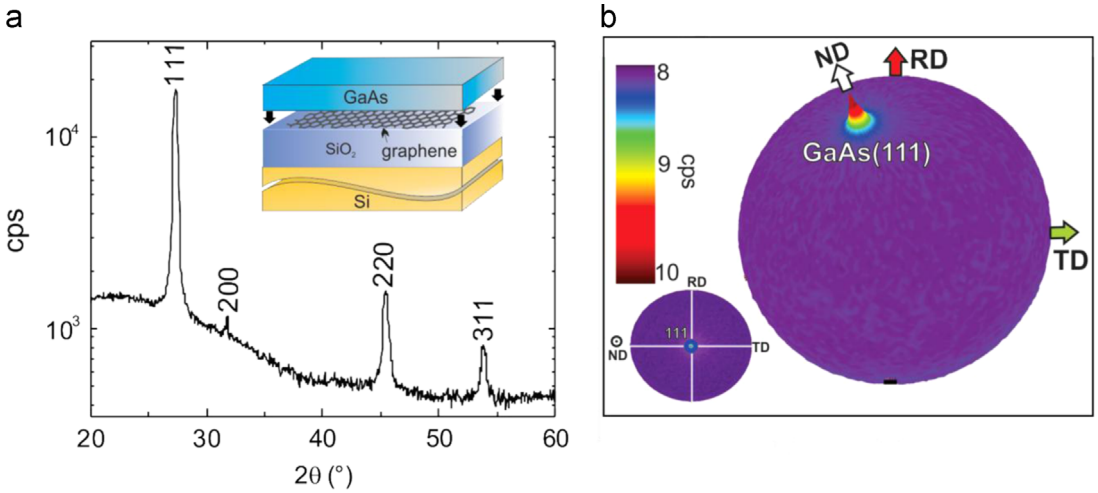

Fig. 5. XRD analysis and pole figure of as-grown GaAs on CVD graphene, (a) HRXRD θ–2θ scan, where multiple peaks correspond to zinc–blende (111), (200), (220) and (311) GaAs. (b) The 3D pole figure of (111) GaAs, showing a preferred orientation of the grown films. The stereographic projection of the (111) pole figure is shown as inset. (For interpretation of the references to color in this figure legend, the reader is referred to the web version of this article.)

incident x-ray diffraction (GIXRD), these slit conditions were used: IS=0.2 mm, H=5.0 mm, RS1=RS2=20.0 mm. The incident beam angle was fixed at 0.3°, while the 2θ arm was scanned from 20° to 60° at speed of 0.3°/min with its step size of 0.05°. As for radial $2\theta/\omega$-scan, the measurement conditions were IS=1.0 mm, H=5 mm, RS=20 mm, while scan speed was 0.5°/min with a step size=0.05°. For both GIXRD and $2\theta/\omega$ measurement, Soller slits were used to reduce the axial divergence of the incident and diffraction x-ray beam to 5°, and a 0.5° parallel slit analyzer (PSA) was used to improve 2θ angular resolution.

The cross-sectional specimen for transmission electron microscopy analysis was prepared by hand polishing using a tripod technique and final thinning using a Gatan precision ion polishing system (PIPS) (Gatan Model 691, operated at 4 keV). The structural characteristics of as-grown GaAs were then investigated using a Tecnai F20, operated at 200 keV.

4. Experimental results

Fig. 4(a) shows the out-of-plane XRD θ–2θ scan pattern for GaAs thin films grown on exfoliated graphite flakes over a 2θ range of 20–70°. The as–grown GaAs films exhibit polycrystalline nature, which is confirmed by (111), (220) and (311) diffraction peaks. Apart from these three film-generating diffraction peaks, the (002) and (004) silicon substrate peaks are observed in the scan. The forbidden Si 002 peak at 2θ=32.9° is attributed to multiple diffractions (Umweganregung). Graphite (002) and (004) reflections are also found as labeled by the red-colored text in Fig. 4(a). The crystalline quality of the thin GaAs film on Ga-terminated graphene was characterized by XRD rocking-curve scans as shown in Fig. 4(b). The FWHM for the rocking curve of the GaAs (111) is 242 arcsec (0.067°), indicating good crystal quality for this orientation (and likely epitaxy). We note that the rocking curves of other surface-normal planes showed broad peaks which is reasonable since our vdW regions covered only a small percentage of an otherwise polycrystalline layer, yielding a strong background signal from the (majority) untemplated regions. The low-temperature grown GaAs on the flakes exhibits a strong (111) preferred-orientation texture. This is an essential step towards demonstration of epitaxy. If larger graphite flakes were used, a clear correlation between the graphene and the fiber texture could be confirmed by a featureless Φ-scan for an asymmetric peak, such as (115). As shown in the inset of Fig. 4(b), the GIXRD 2θ scan exhibits peaks at the expected locations for GaAs films, corresponding to the GaAs (111), (220), and (311), which indicates that the as-grown material is randomly oriented

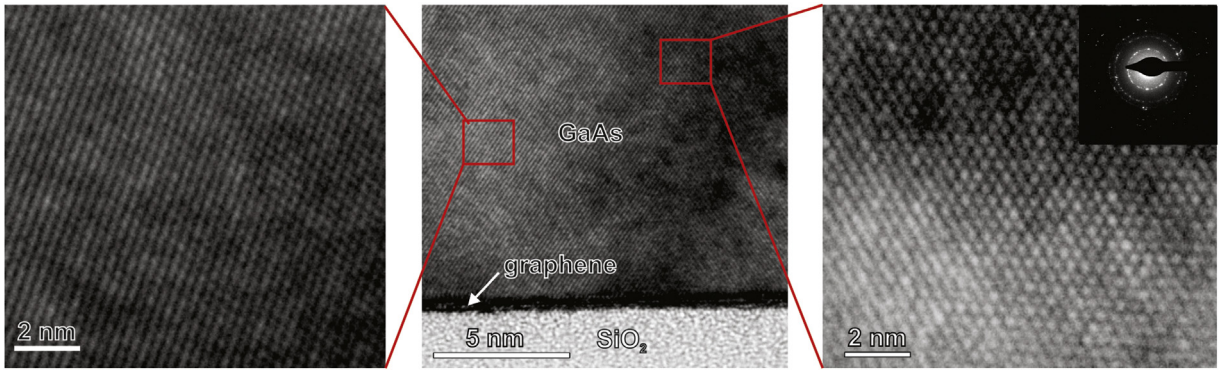

Fig. 6. Cross-sectional TEM image near the interface between GaAs film and CVDgraphene/SiO_2. Magnified TEM images of the solid red-square areas. To maximize ease of interpretation, the film growth direction is along the vertical direction of images. The corresponding SAED ring pattern is shown as inset.

polycrystalline. Note that there are two strong unlabeled peaks at $2\theta = 53^\circ$ and 56.3° for these samples which could be due to graphitic regions.

To assess the quality of as-grown film and to benchmark our results, the full width at half-maximum (FWHM) of the XRD rocking curve could be compared with the prior reports of FWHM values obtained from GaAs on Si using conventional direct heteroepitaxy. By employing several direct growth approaches [17–20], micron thick buffer layer was deposited on silicon in order to obtain a FWHM value as low as 242 arcsec. However, the as-grown GaAs film via vdWE achieves the same FWHM with film thicknesses on the order of 25 nm. The two orders of magnitude improvement in the quality of our GaAs films can be attributed to the graphene buffer layer mitigating lattice and thermal mismatch between GaAs and the underlying substrate.

To verify crystalline quality of the material, the out-of-plane XRD θ–2θ scan pattern was performed for GaAs films grown on large-area CVD graphene over a 2θ range of 20–60°. As shown in Fig. 5(a), the θ–2θ scan is composed of ZB (111), (200), (220) and (311) GaAs peaks with unequal intensities. Therefore, the as-grown GaAs film on CVD graphene is confirmed to be polycrystalline.

The pole-figure has been proven to be one of the most powerful XRD techniques for studying texture in thin films. The strong (111) peak at the center of the pole figure as shown in 3D representation of Fig. 5(b) indicates that the as–grown films are preferably (111)-oriented along the surface normal. Also, the stereographic projection format of such pole figure is shown as an inset in Fig. 5(b). The FWHM of the surface normal peak and the degree of the preferred orientation are calculated to be 1.5° and 2.2%, suggesting strong fiber texture in the GaAs films. In a previous study, it was reported that (111) orientation is highly favored by the underlying graphene layer, exhibiting a triangular lattice symmetry. It should be noted that the XRD θ–2θ scan and pole figure data reported here were collected from the sample where the GaAs growth was performed on a blanket graphene layer sitting on SiO_2/(111)-oriented silicon substrates. This clearly suggests that the silicon substrate will have a negligible influence in defining the orientation of the grown layer.

Selected area electron diffraction (SAED) patterns obtained from the GaAs layer grown on CVD-graphene/SiO_2/Si contain a series of rings, which indicates the presence of a polycrystalline material. Using the diffraction pattern of the single crystal Si substrate as a reference, the lattice plane spacings of the diffraction pattern and the relative intensity of the diffraction rings suggest that a majority of GaAs is grown in the cubic ZB phase. Fig. 6 shows a high-resolution lattice image of an approximately 100 nm thick GaAs layer containing two grains in which a ⟨110⟩ direction is aligned close to parallel to the electron beam (see enlarged areas). The lattice fringe patterns observed are consistent with these grains being ZB in structure which is in good agreement with the theoretical findings. Defects such as microtwins and stacking faults were observed within some of the grains. The typical grain size observed in an approximately 100 nm think GaAs layer was between 20 and 60 nm.

5. Conclusion

In summary, we have reported the detailed theoretical and experimental characterization of MBE-grown GaAs thin films on graphene/silicon substrates using quasi-van der Waals epitaxy, which provides novel insights into the quality of grown material. From the theoretical study, we conclude that graphene as a buffer layer is more suitable than h-BN and MoS_2 in the case of the growth of 3D materials on 2D layered surfaces. By XRD measurements, it is verified that our as-grown GaAs films on graphene/silicon exhibit the polycrystalline nature with a strong [111]-oriented fiber texture. In the study of the GaAs/graphene heterointerface, GaAs ZB crystal structure is experimentally found to be more stable than WZ GaAs, providing good agreement with the theoretical predictions. Since the CVDgrown graphene itself is polycrystalline, the as-grown materials on top of this 2D buffer layer cannot be single-crystalline. Therefore, future efforts will mainly focus on using single-domain graphene as a buffer layer, leading to single-crystalline GaAs which will serve as a potential and cost-effective route towards heteroepitaxial integration of GaAs on silicon in the developing field of silicon photonics.

Acknowledgment

We would like to acknowledge the collaboration of this research with King Abdul-Aziz City for Science and Technology (KACST) via The Center of Excellence for Nanotechnologies (CEGN). D.W. and R.K.L acknowledge the support from FAME, one of six centers of STARnet, a semiconductor Research Corporation Program sponsored by MARCO and DARPA. This work used the Extreme Science and Engineering Discovery Environment (XSEDE), which is supported by National Science Foundation Grant number OCI-1053575.

References

[1] A. Koma, K. Sunouchi, T. Miyajima, Microelectron. Eng. 2 (1984) 129.
[2] T. Ueno, H. Yamamoto, K. Saiki, A. Koma, Appl. Surf. Sci. 113–114 (1997) 33.
[3] J. Kim, C. Bayram, H. Park, C.W. Cheng, C. Dimitrakopoulos, J.A. Ott, K.B. Reuter, S.W. Bedell, D.K. Sadana, Nat. Commun. 5 (2014) 4836.
[4] A.M. Munshi, D.L. Dheeraj, V.T. Fauske, D.C. Kim, A.T. van Helvoort, B. O. Fimland, H. Weman, Nano Lett. 12 (2012) 4570.

[5] C.-P. Chu, S. Arafin, T. Nie, K. Yao, X. Kou, L. He, C.-Y. Wang, S.-Y. Chen, L.-J. Chen, S.M. Qasim, M.S. BenSaleh, K.L. Wang, Cryst. Growth Des. 14 (2014) 593.
[6] C.-P. Chu, S. Arafin, G. Huang, T. Nie, K.L. Wang, Y. Wang, J. Zou, S.M. Qasim, M. S. BenSaleh, J. Vac. Sci. Technol. B 32 (2014) 02C111.
[7] K.S. Novoselov, Z. Jiang, Y. Zhang, S.V. Morozov, H.L. Stormer, U. Zeitler, J. C. Maan, G.S. Boebinger, P. Kim, A.K. Geim, Science 315 (2007) 1379.
[8] C.H. Lee, Y.J. Kim, Y.J. Hong, S.R. Jeon, S. Bae, B.H. Hong, G.C. Yi, Adv. Mater. 23 (2011) 4614.
[9] P.K. Mohseni, A. Behnam, J.D. Wood, C.D. English, J.W. Lyding, E. Pop, X. Li, Nano Lett. 13 (2013) 1153.
[10] A.M. Munshi, H. Weman, Phys. Status Solidi 7 (2013) 713.
[11] S. Arafin, X. Liu, Z. Mi, J. Nanophotonics 7 (2013) 074599.
[12] Y. Alaskar, S. Arafin, D. Wickramaratne, M.A. Zurbuchen, L. He, J. McKay, Q. Lin, M.S. Goorsky, R.K. Lake, K.L. Wang, Adv. Funct. Mater. 24 (2014) 6629.
[13] G. Kresse, J. Hafner, Phys. Rev. B 47 (1993) 558.
[14] S. Grimme, J. Comput. Chem. 27 (2006) 1787.
[15] X. Shi, Q. Yin, Y. Wei, Carbon 50 (2012) 3055.
[16] Y. Zhan, Z. Liu, S. Najmaei, P.M. Ajayan, J. Lou, Small 8 (2012) 966.
[17] M.E. Groenert, C.W. Leitz, A.J. Pitera, V. Yang, H. Lee, R.J. Ram, E.A. Fitzgerald, J. Appl. Phys. 93 (2003) 362.
[18] Y. Takano, M. Hisaka, N. Fujii, K. Suzuki, K. Kuwahara, S. Fuke, Appl. Phys. Lett. 73 (1998) 2917.
[19] K. Nozawa, Y. Horikoshi, Jpn. J. Appl. Phys. 30 (1991) 668.
[20] M. Tamura, T. Yodo, T. Saitoh, J. Palmer, J. Cryst. Growth 150 (1995) 654.

Please cite this article as: Y. Alaskar, et al., Journal of Crystal Growth (2015), http://dx.doi.org/10.1016/j.jcrysgro.2015.02.003